

Selected Paper

Magnetic Ordering in Organic-Radical Assemblies

Masashi Hatanaka* and Ryuichi Shiba

Department of Materials and Life Sciences, Graduate School of Advanced Science & Technology, Tokyo Denki University, 2-2 Kanda Nishiki-cho, Chiyoda-ku, Tokyo 101-8457

Received February 5, 2008; E-mail: mhatanaka@xug.biglobe.ne.jp

Ferromagnetic interactions in three-dimensionally stacked organic-radical assemblies were deduced under periodic boundary conditions. Although the topological-linkage patterns apparently contained pentavalent carbon atomic sites due to the three dimensionalities, it was shown that the degenerate non-bonding crystal orbitals (NBCOs) were subject to orbital mixing to form Wannier-transformed NBCOs, analogous to non-Kekulé polymers. In the ferromagnetic π–π stacking modes, the NBCOs were spread over more than two adjacent unit cells. On the other hand, in the π–π antiferromagnetic stacking modes, the NBCOs were localized only at one unit cell. High-spin preferences in the ferromagnetic stacking modes were attributed to anti-parallel-spin instabilities in effective two-electron wave functions consisting of products of NBCOs (PNBCOs). Our analysis was confirmed by theoretical calculations.

Organic-radical assemblies with three-dimensional π–π stacking modes are promising candidates for molecular ferromagnets. In 1963, McConnell proposed high-spin criterion of organic-radical assemblies based on Heisenberg Hamiltonian:[1]

$$H^{AB} = -\mathbf{S}^A \cdot \mathbf{S}^B \sum_{i,j} J_{ij}^{AB} \sigma_i^A \sigma_j^B \quad (J_{ij}^{AB} < 0) \tag{1}$$

where $\mathbf{S}^A$ and $\mathbf{S}^B$ are spin operators of molecule A and B, respectively, and J_{ij}^{AB} is the exchange integral. J_{ij}^{AB} is negative in usual organic compounds, as is based on valence bond theory.[2] σ_i^A and σ_j^B are spin densities at the i-th site in molecule A and the j-th site in molecule B, respectively. That is, spatially stacked spin-polarized π systems are predicted to be ferromagnetic when spin-density products become negative as much as possible. Then, the Hamiltonian in eq 1 is minimized. This means that spin polarization is expected at each adjacent carbon atomic site in organic-radical assemblies. **1** and **2** in Figure 1 are two possible ferromagnetic stacking modes of allyl-radical dimer, which is the simplest organic-radical assembly. The conformational parameters are also shown. Both in **1** and **2**, the carbon atomic sites are combined between so-called starred atoms and unstarred atoms. Within valence bond theory, up and down spins are induced on starred and unstarred atoms, respectively. **1** has two linking point of starred and unstarred atoms, as shown by the dashed lines in Figure 1. High-spin stability in **1** has been established by the unrestricted Hartree–Fock (UHF) method, in which spin-polarization effects are well described.[3] **2** has only one linking point of starred and unstarred atoms, as shown in Figure 1. To our knowledge, spin states in **2** have not been studied in detail, but it is worthwhile to clarify the spin states of **2** in that this is considered to be another ferromagnetic isomer of allyl-radical dimer. McConnell's proposal has been applied to more complicate systems such as diphenylcarbene oligomers and/or polymers,[4,5] of which high-spin states have been experimentally established.[6–8]

Although McConnell's proposal is based on valence bond theory, there have been some attempts to complement this prediction in view of molecular orbital methods.[9,10] That is, high-spin stabilities in organic-radical assemblies have been attributed to degeneracy of non-bonding molecular orbitals (NBMOs) and Hund's rule. Figure 2 shows amplitude pattern of NBMOs in **1** and **2**, respectively. In the dimers, there are two NBMOs originated from an allyl radical. Each NBMO of allyl-radical moiety has nodes at the central carbon atomic sites, and thus, two NBMOs in the dimers are not overlapped with each other. Then, two NBMOs are degenerate, and thus, lead to triplet stabilities due to Hund's rule. Thus, McConnell's proposal has been complemented in view of the non-overlapping interactions between NBMOs.[9,10]

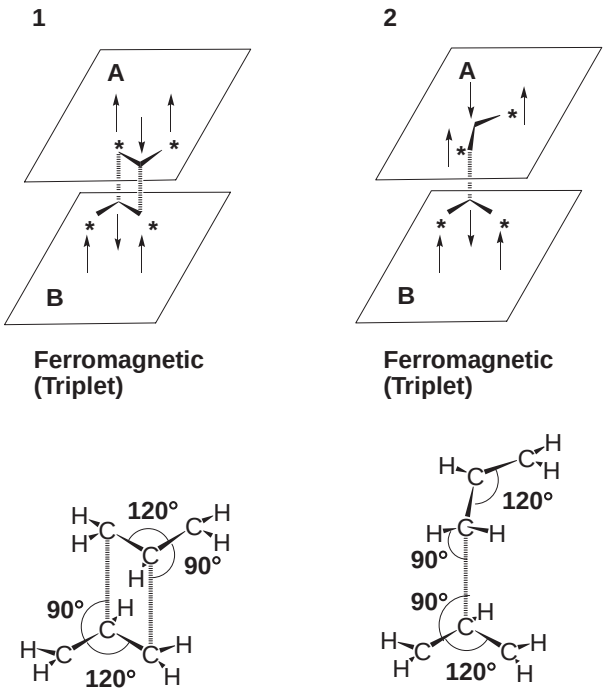

Figure 1. Molecular structures of allyl-radical assemblies. Both **1** and **2** are ferromagnetic stacking modes.

Published on the web August 11, 2008; doi:10.1246/bcsj.81.966

Figure 2. Non-overlapping interactions between two non-bonding molecular orbitals (NBMOs) of **1** and **2**.

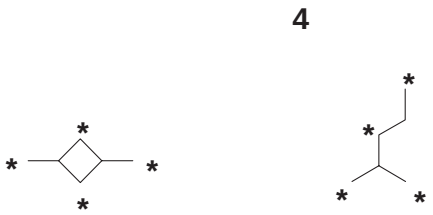

Figure 3. Molecular structures of non-Kekulé biradicals 1,3-dimethylenecyclobutadiene (**3**) and 1,1-dimethylene-1,3-butadiene (**4**).

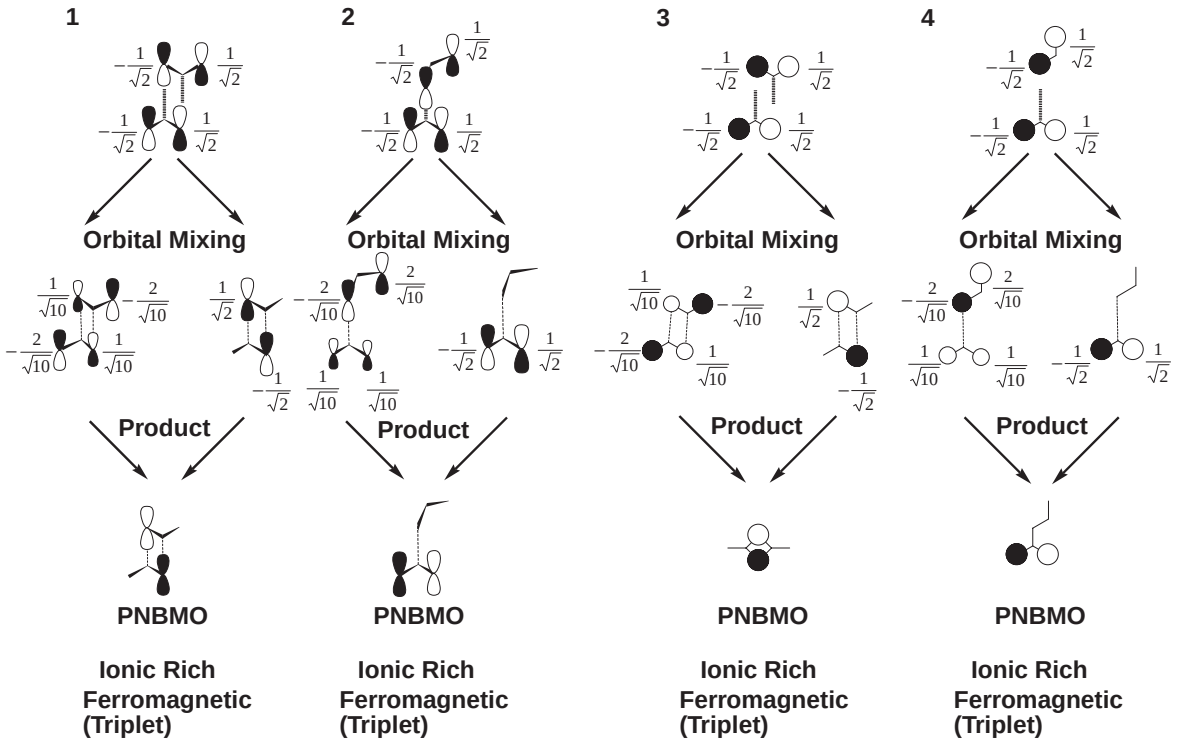

Figure 4. Orbital-mixing patterns in **1**, **2**, **3**, and **4**. These molecules are triplet stable due to the ionic character in the product of NBMOs (PNBMOs).

However, in order to deduce high-spin states in NBMO-degenerate systems, orbital mixing between NBMOs should be taken into account, because NBMOs are not uniquely determined due to degeneracy. The possibility of orbital mixing in NBMO-degenerate systems has been pointed out in so-called disjoint/nondisjoint biradicals including non-Kekulé biradicals by Aoki and Imamura.[11] Moreover, it has been shown that NBMOs in disjoint/nondisjoint biradicals and/or polyradicals should be localized as much as possible so that the exchange integrals are minimized.[11–13] Such NBMOs are called "localized NBMOs." In the case of non-Kekulé biradicals, the localized NBMOs are obtained by unitary transformations of corresponding canonical orbitals.[11] Therefore, in organic-radical assemblies, we should also construct localized NBMOs instead of usual NBMOs, analogous to non-Kekulé biradicals. Localized NBMOs in three-dimensionally stacked organic-radical assemblies also seems to be determined uniquely by unitary transformation, because linkage patterns of the carbon atomic sites resemble those of non-Kekulé systems.

That is, in the present case, molecular skeletons of **1** and **2** resemble those of non-Kekulé biradical 1,3-dimethylenecyclobutadiene (**3** in Figure 3) and 1,1-dimethylene-1,3-butadiene (**4** in Figure 3), respectively. Both **3** and **4** are nondisjoint biradicals with triplet ground states.[14,15] Therefore, the orbital mixing patterns and resultant localized NBMOs in **1** and **2** are obtained by comparing them with those in **3** and **4**, respectively. This situation is schematically shown in Figure 4. The canonical-type NBMOs are mixed by proper unitary transformations[11] to form localized NBMOs, and resultant product PNBMOs (product of NBMOs) become rich in ionic terms due to the nondisjoint character. PNBMOs are effective two-electron wave functions consisting of product of NBMOs,[16] as explained below.

In nondisjoint biradicals, the high-spin stabilities have been rationalized to anti-parallel-spin instabilities in PNBMOs.[16] PNBMO is defined as follows:

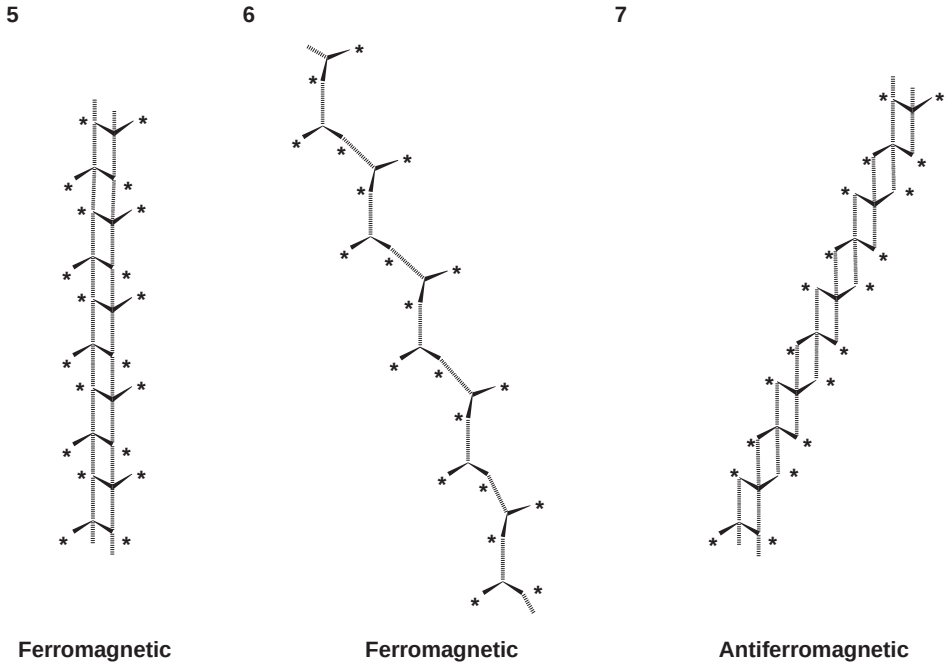

Figure 5. Molecular structures of poly(allyl radical) assemblies. **5** and **6** are ferromagnetic, and **7** is antiferromagnetic.

$$\phi_i = \sum_r C_{ri}\chi_r \tag{2}$$

$$\phi_j = \sum_s C_{sj}\chi_s \tag{3}$$

$$PNBMO_{i,j} = \phi_i(\boldsymbol{1})\phi_j(\boldsymbol{2}) = \sum_r \sum_s C_{ri}C_{sj}\chi_r(\boldsymbol{1})\chi_s(\boldsymbol{2})$$

$$\cong C\sum_r C_{ri}C_{rj}\chi_r(\boldsymbol{1})\chi_r(\boldsymbol{2}) \tag{4}$$

where C_{ri} and C_{sj} are Hückel-molecular-orbital coefficients on the carbon atomic site r and s in NBMO ϕ_i and ϕ_j, respectively. χ represents $2p_z$ carbon atomic orbitals. The electron numbers ***1*** and ***2*** are added for clarity. The summation includes all carbon atomic sites. The differential overlaps were neglected in the approximation (NDO approximation). The NDO approximation is adequate for the present purpose. Here, we apply the PNBMO concept for explanation of triplet stabilities of **1**, **2**, **3**, and **4**. The localized NBMOs of **1**, **2**, **3**, and **4** span common atoms, and thus, PNBMOs contain ionic terms within the Hückel molecular orbital method. Again, this is schematically seen from Figure 4. Then, resultant simultaneous occupancy of two electrons at the same carbon atomic site leads to singlet instabilities due to the Pauli principle. This is the origin of the triplet stabilities of **1**, **2**, **3**, and **4**. Intuitively, the PNBMOs of **1** and **2** are obtained by comparing the molecular structures of them with **3** and **4**, because topological linkages of **1** and **2** are identical to those in **3** and **4**.

Based on the perspective above, we can also expect orbital mixing and localization in organic-radical extended systems, in which organic radicals are stacked through three-dimensional π–π interactions. **5** in Figure 5 is an extended system of **1**, of which high-spin state and spin-polarization effect also have been established by analyzing the corresponding oligomers.[3] This is a ladder-like polymer of which point group belongs to C_i. **6** is an extended system of **2**, in which starred atoms and unstarred atoms are connected only by one linking point per unit cell. The point group belongs to C_1 (asymmetry). From the McConnell prediction, this is also considered to be ferromagnetic due to the spin-polarization rule. The high-spin stability of this polymer is theoretically deduced later. **7** is another type of extended systems of **1**, of which the linking mode is different from **5**. The point group belongs to C_i. Intuitively, this polymer also seems to be ferromagnetic, because a spin-polarization structure can be formally drawn, similar to **5**. However, as is shown later, this is not a ferromagnetic but an antiferromagnetic polymer, contradictory to the spin-polarization rule. Thus, the spin-polarization rule is inadequate to distinguish magnetic properties of organic-radical assemblies. We propose that the origin of magnetic ordering in the π–π stacking modes result from anti-parallel-spin instabilities in effective two-electron wave functions consisting of products of non-bonding crystal orbitals (NBCOs) rather than the simple spin-polarization rule.

In this paper, we present a simple method to distinguish ground-state spin states of organic-radical assemblies based on a Hückel-like molecular orbital method. We show that NBMOs or NBCOs in organic-radical assemblies are subject to orbital mixing to form localized three-dimensional NBMOs or NBCOs. In particular, in extended systems, NBCOs form Wannier functions, similar to non-Kekulé polymers. Whereas in the ferromagnetic stacking modes, the Wannier functions are spread over more than two adjacent unit cells, in the antiferromagetic stacking modes, the Wannier functions are localized only at one unit cell. High-spin preferences in the ferromagnetic stacking modes were attributed to anti-parallel-spin instabilities in effective two-electron wave functions consisting of products of NBCOs (PNBCOs), similar to non-Kekulé polymers.[17,18] Our analysis is confirmed by theoretical calculations.

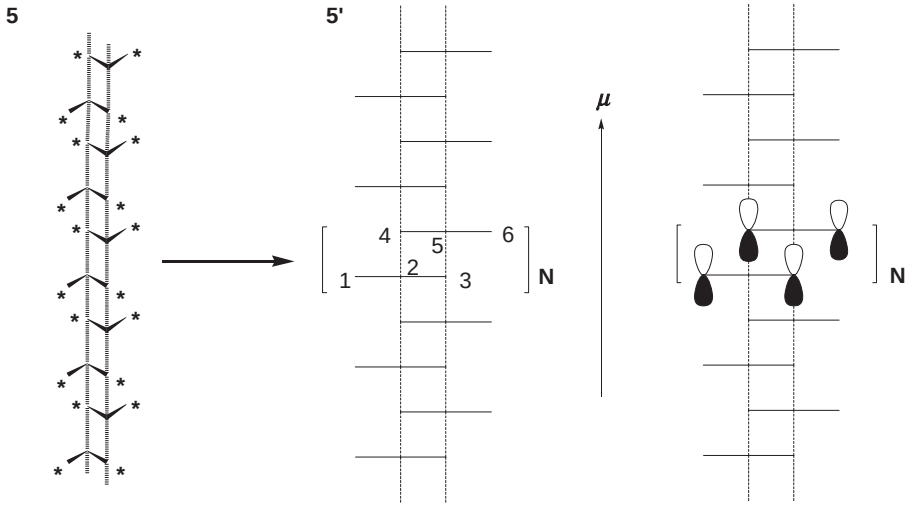

Figure 6. Carbon atomic linkage in **5**. The skeleton of **5** is formally reduced as **5′**.

Theoretical

Allyl-Radical Dimers. Before we discuss the magnetic ordering of the extended systems, the relationships between exchange integrals and NBMOs coefficients are explained by analyzing the dimer models. As is described above, topological linkage of carbon atomic sites in allyl-radical dimers **1** and **2** resemble those in triplet biradicals **3** and **4**, respectively.

Here, we consider exchange integrals of **1** and **2** comparing them with those in non-Kekulé biradicals **3** and **4**. In the case of non-Kekulé biradicals including **3** and **4**, exchange integrals K_{ij} between two NBMOs are approximately proportional to the L_{ij} index, which has been introduced by Aoki and Imamura:[11]

$$\begin{aligned} K_{ij} &= \iint \phi_i(\boldsymbol{1})\phi_j(\boldsymbol{1})\frac{e^2}{r_{12}}\phi_i(\boldsymbol{2})\phi_j(\boldsymbol{2})\mathrm{d}\tau_1\mathrm{d}\tau_2 \\ &= \sum_r\sum_s\sum_t\sum_u C_{ri}C_{sj}C_{ti}C_{uj}(rs|tu) \\ &\cong \sum_r C_{ri}^2C_{rj}^2(rr|rr) \propto \sum_r C_{ri}^2C_{rj}^2 = L_{ij} \end{aligned} \tag{5}$$

where $(rs|tu)$ is the electron-repulsion integral with only one-centered integrals taken into account. C_{ri} and C_{rj} are coefficients on the r-th carbon atomic sites in the i-th and j-th localized NBMOs, respectively. From eqs 2–4, we see that L_{ij} index is identical to the square of norm in PNBMOs, that is, sum of the squared amplitudes of PNBMOs.[16] Therefore, in **3** and **4**, we can image from Figure 4 that the simple products between the coefficients on the same carbon atomic sites of each NBMO becomes $C_{ri}C_{rj}$, and the sum of the their squares $C_{ri}{}^2C_{rj}{}^2$ is approximately proportional to the exchange integrals.

In the same manner, exchange integrals in ally-radical dimers **1** and **2** are considered to be qualitatively proportional to the sum of the square amplitude of PNBMOs coefficients. Apart from the orientation of the $2p_z$ carbon atomic orbitals, the exchange integrals are also approximately proportional to $C_{ri}{}^2C_{rj}{}^2$, where C_{ri} and C_{rj} are also localized-NBMOs coefficients. Thus, exchange integrals in organic-radical dimers are also rationalized to NBMOs coefficients, analogous to non-Kekulé biradicals.

Allyl-Radical Polymers. Next, we consider allyl-radical polymers **5**, **6**, and **7** (Figure 5). These are extended systems of ally-radical dimers. In extended systems, we need to construct localized NBCOs instead of localized NBMOs. In the case of non-Kekulé polymers, the method for construction of localized NBCOs has been established under one-dimensional[17] and two-dimensional[18] periodic boundary conditions by using Wannier transformation. Moreover, the high-spin stabilities in non-Kekulé polymers have been attributed to anti-parallel-spin instabilities in effective two-electron wave function *PNBCOs*. Analogous to non-Kekulé polymers, NBCOs in organic-radical assemblies should be subject to orbital mixing, because the NBCOs are also degenerate. Considering the perspective described above, we adopt Wannier-transformed NBCOs, which are localized expressions of Bloch-type NBCOs. The method for construction of Wannier-transformed NBCOs follows.

We first show that topological linkage of carbon atomic sites of **5** is reduced to the non-Kekulé-like skeleton **5′** as described in Figure 6. In Figure 6, only carbon atomic sites are shown. The skeleton apparently resembles those in non-Kekulé polymers in that terminal methylene groups are radical centers. Strictly speaking, **5′** is not a non-Kekulé skeleton, because it apparently contains pentavalent carbon atoms at the unstarred atoms. However, we can perform simple Hückel-like molecular orbital analysis on **5** by focusing only on the purely topological linkage **5′**, as described below.

We define the unit cell of **5′** as described in Figure 6. The unit cell contains two allyl-radical moieties. The numbers 1–6 in the unit cell are indices of the carbon atomic sites. N represents the number of unit cells, and $\boldsymbol{\mu}$ is the lattice vector. Here, we construct Bloch functions of **5′**. We focus only on the non-bonding Bloch functions. In the present case, the Bloch functions are created by non-bonding $2p_z$ atomic orbitals, similar to non-Kekulé polymer. However, our treatment in **5** is different from usual crystal orbital methods in that the $2p_z$ atomic orbitals as basis set are oriented not perpendicular but parallel to the lattice vector $\boldsymbol{\mu}$. The orientation of the $2p_z$ atomic orbitals is also schematically shown in Figure 6. In Figure 6, the $2p_z$ atomic orbitals are symbolically depicted on-

ly on the starred atoms, similar to usual non-Kekulé systems. Then, the $2p_z$ atomic orbitals in **5** form quasi NBCOs, similar to non-Kekulé chain polymers. Thus, we can formally deduce the Bloch functions of **5** by solving the Hückel-type secular equation. Although the Coulomb and resonance integrals are different from the usual Hückel method, we can construct the approximately non-bonding bands by focusing only on the zero-energy dispersions.

The Bloch function φ_k is generally expressed by using NBCOs coefficients $C_r(k)$, which depend on wavenumber k running $-\pi$ to π:

$$\varphi_k = \frac{1}{\sqrt{N}} \sum_{\mu}^{N} \sum_{r}^{n} \exp(ik\mu) C_r(k) \chi_{\mu,r} \tag{6}$$

where μ and r are indices of a unit cell and atomic orbitals therein, respectively. N and n are number of unit cells and atomic orbitals therein, respectively. χ represents the $2p_z$ atomic orbitals. In the case of **5**, r runs 1 to 6. The NBCOs coefficients $C_r(k)$ are obtained by solving the secular equation as follows:

$$\begin{vmatrix} x & 1 & 0 & 0 & 0 & 0 \\ 1 & x & 1 & 1+e^{ik} & 0 & 0 \\ 0 & 1 & x & 0 & 1+e^{ik} & 0 \\ 0 & 1+e^{-ik} & 0 & x & 1 & 0 \\ 0 & 0 & 1+e^{-ik} & 1 & x & 1 \\ 0 & 0 & 0 & 0 & 1 & x \end{vmatrix} = 0 \tag{7}$$

where x is:

$$x = \frac{\alpha - \varepsilon}{\beta} \tag{8}$$

α and β are Coulomb and resonance integral, respectively. ε is orbital energy.

The NBCOs correspond to the dispersion with $x = 0$. In the case of **5**, the NBCO bands are doubly degenerate, because there are two radical centers in the unit cell. As the NBCOs coefficients $C_r(k)$, we obtained two linear-independent roots $C_{r,a}(k)$ and $C_{r,b}(k)$:

$$C_{1,a}(k) = \frac{1}{\sqrt{2}} \left(-\frac{2+e^{ik}}{2\sqrt{3+2\cos k}} + \frac{1}{2}\cos k \right),$$

$$C_{1,b}(k) = \frac{1}{\sqrt{2}} \left(-\frac{2+e^{ik}}{2\sqrt{3+2\cos k}} - \frac{1}{2}\cos k \right) \tag{9}$$

$$C_{2,a}(k) = C_{5,a}(k) = 0, \quad C_{2,b}(k) = C_{5,b}(k) = 0 \tag{10}$$

$$C_{3,a}(k) = \frac{1}{\sqrt{2}} \left(\frac{1}{2\sqrt{3+2\cos k}} + \frac{1}{2} \right),$$

$$C_{3,b}(k) = \frac{1}{\sqrt{2}} \left(\frac{1}{2\sqrt{3+2\cos k}} - \frac{1}{2} \right) \tag{11}$$

$$C_{4,a}(k) = \frac{1}{\sqrt{2}} \left(\frac{1}{2\sqrt{3+2\cos k}} - \frac{1}{2} \right),$$

$$C_{4,b}(k) = \frac{1}{\sqrt{2}} \left(\frac{1}{2\sqrt{3+2\cos k}} + \frac{1}{2} \right) \tag{12}$$

$$C_{6,a}(k) = \frac{1}{\sqrt{2}} \left(-\frac{2+e^{-ik}}{2\sqrt{3+2\cos k}} - \frac{1}{2}\cos k \right),$$

$$C_{6,b}(k) = \frac{1}{\sqrt{2}} \left(-\frac{2+e^{-ik}}{2\sqrt{3+2\cos k}} + \frac{1}{2}\cos k \right) \tag{13}$$

where "a" and "b" are indices of the two bands.

Since $C_r(k)$ generally becomes a complex number, we adopt the real part as follows:

$$C'_r(k) = \frac{1}{2}\{C_r(k) + C_r(k)^*\} = \frac{1}{2}\{C_r(k) + C_r(-k)\} \tag{14}$$

where $C_r(k)^*$ is the complex conjugate of $C_r(k)$. This procedure guarantees even-function character of Wannier functions, which is applied later. The imaginary parts do not contribute to the Wannier-function coefficients.

The Wannier functions are generally expressed by using the following transformation:[19]

$$\psi_\nu = \sum_{\mu}^{N} \sum_{r}^{n} a_r(\mu - \nu) \chi_{\mu,r} \tag{15}$$

where $a_r(\mu - \nu)$ is:

$$a_r(\mu - \nu) = \frac{1}{2\pi} \int_{-\pi}^{\pi} \exp\{i(\mu - \nu)k\} C'_r(k) \mathrm{d}k \tag{16}$$

in the limit of $N \to \infty$.

The coefficient $a_r(\mu - \nu)$ depends on only the difference $(\mu - \nu)$. We express $(\mu - \nu)$ as τ:

$$\tau = \mu - \nu \tag{17}$$

τ is difference between the unit-cell number μ and ν.

In the present case, there are two Wannier functions $a_{r,a}(\tau)$ and $a_{r,b}(\tau)$ corresponding to $C_{r,a}(k)$ and $C_{r,b}(k)$, respectively. $a_{r,a}(\tau)$ and $a_{r,b}(\tau)$ satisfied following relations:

$$a_{1,a}(\tau) = \frac{1}{\sqrt{2}} \Bigg[-2a_{3,a}(\tau) - \frac{1}{2}\{a_{3,a}(\tau+1) + a_{3,a}(\tau-1)\} + \frac{1}{4}(\delta_{\tau+1+\nu,\nu} + \delta_{\tau-1+\nu,\nu}) \Bigg],$$

$$a_{1,b}(\tau) = \frac{1}{\sqrt{2}} \Bigg[-2a_{3,b}(\tau) - \frac{1}{2}\{a_{3,b}(\tau+1) + a_{3,b}(\tau-1)\} - \frac{1}{4}(\delta_{\tau+1+\nu,\nu} + \delta_{\tau-1+\nu,\nu}) \Bigg] \tag{18}$$

$$a_{2,a}(\tau) = a_{5,a}(\tau) = 0, \quad a_{2,b}(\tau) = a_{5,b}(\tau) = 0 \tag{19}$$

$$a_{3,a}(\tau) = \frac{1}{\sqrt{2}} \left[\frac{1}{2\pi} \int_{-\pi}^{\pi} \frac{\cos(\tau k)}{2\sqrt{3+2\cos k}} \mathrm{d}k + \frac{1}{2}\delta_{\tau+\nu,\nu} \right],$$

$$a_{3,b}(\tau) = \frac{1}{\sqrt{2}} \left[\frac{1}{2\pi} \int_{-\pi}^{\pi} \frac{\cos(\tau k)}{2\sqrt{3+2\cos k}} \mathrm{d}k - \frac{1}{2}\delta_{\tau+\nu,\nu} \right] \tag{20}$$

$$a_{4,a}(\tau) = \frac{1}{\sqrt{2}} \left[\frac{1}{2\pi} \int_{-\pi}^{\pi} \frac{\cos(\tau k)}{2\sqrt{3+2\cos k}} \mathrm{d}k - \frac{1}{2}\delta_{\tau+\nu,\nu} \right],$$

$$a_{4,b}(\tau) = \frac{1}{\sqrt{2}} \left[\frac{1}{2\pi} \int_{-\pi}^{\pi} \frac{\cos(\tau k)}{2\sqrt{3+2\cos k}} \mathrm{d}k + \frac{1}{2}\delta_{\tau+\nu,\nu} \right] \tag{21}$$

$$a_{6,a}(\tau) = \frac{1}{\sqrt{2}} \Bigg[-2a_{3,a}(\tau) - \frac{1}{2}\{a_{3,a}(\tau+1) + a_{3,a}(\tau-1)\} - \frac{1}{4}(\delta_{\tau+1+\nu,\nu} + \delta_{\tau-1+\nu,\nu}) \Bigg],$$

$$a_{6,b}(\tau) = \frac{1}{\sqrt{2}} \Bigg[-2a_{3,b}(\tau) - \frac{1}{2}\{a_{3,b}(\tau+1) + a_{3,b}(\tau-1)\} + \frac{1}{4}(\delta_{\tau+1+\nu,\nu} + \delta_{\tau-1+\nu,\nu}) \Bigg] \tag{22}$$

where $\delta_{\tau+\nu,\nu}$ is Kronecker's delta. These relations were deduced by using the addition theorem of cosine functions.

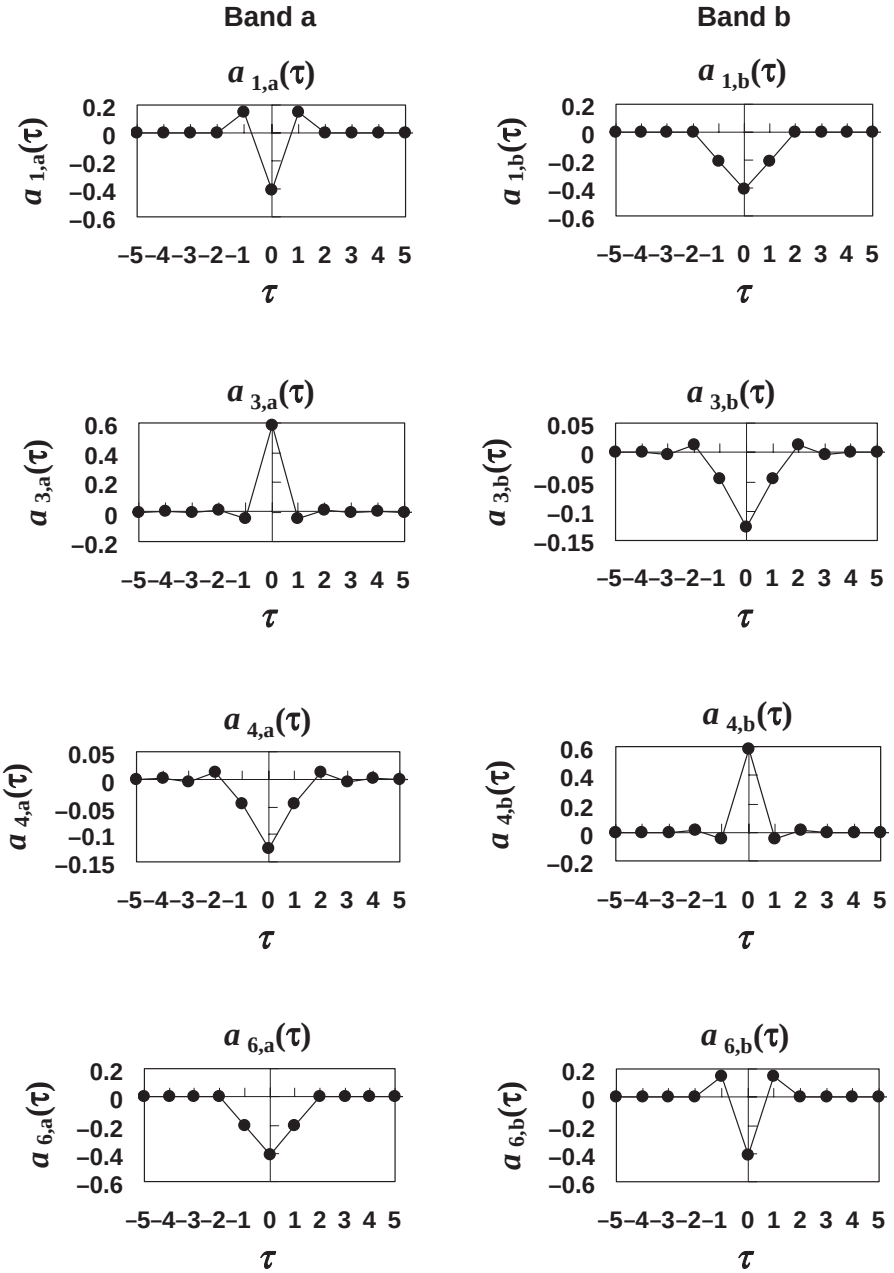

Figure 7. Wannier-function coefficients in **5**.

We note that all the $a_r(\tau)$ are even functions with respect to τ, that is,

$$a_r(\tau) = a_r(-\tau) \tag{23}$$

This is guaranteed by eq 14.

Here, we describe degree of localization in each Wannier function. The ν-th Wannier function is localized only at $(\nu \pm 1)$-th cells. For example, τ dependence of $a_{r,a}(\tau)$ and $a_{r,b}(\tau)$ in **5** were shown in Figure 7. We can see that $a_{r,a}(\tau)$ and $a_{r,b}(\tau)$ ($r = 1$, 3, 4, and 6) decreases when the absolute value of τ increases. That is:

$$\begin{aligned} 0 < \cdots |a_r(-3)| < |a_r(-2)| \ll |a_r(-1)| < |a_r(0)| \\ > |a_r(1)| \gg |a_r(2)| > |a_r(3)| \cdots > 0 \end{aligned} \tag{24}$$

In particular, $a_r(\tau)$ with $|\tau| > 2$ were trivial compared with $a_r(0)$ and $a_r(1)$. Therefore, we supposed that:

$$a_r(\tau) = 0 \text{ when } |\tau| \geq 2 \tag{25}$$

This situation was schematically illustrated in Figure 8. For example, the ν-th Wannier function ψ_ν is spread over the $(\nu \pm 1)$-th cells. Similarly, the $(\nu + 1)$-th Wannier function $\psi_{\nu+1}$ is spread over the $\{(\nu + 1) \pm 1\}$-th cells. Then, ψ_ν and $\psi_{\nu+1}$ span common atoms between the ν-th and $(\nu + 1)$-th cells expressed by shadow. As is shown later, such common-spanned regions between ν-th and $(\nu + \delta)$-th Wannier functions is formulated as effective two-electron wave function $PNBCO_{\nu,\nu+\delta}$, and play an important role in ferromagnetic interactions in organic-radical assemblies.

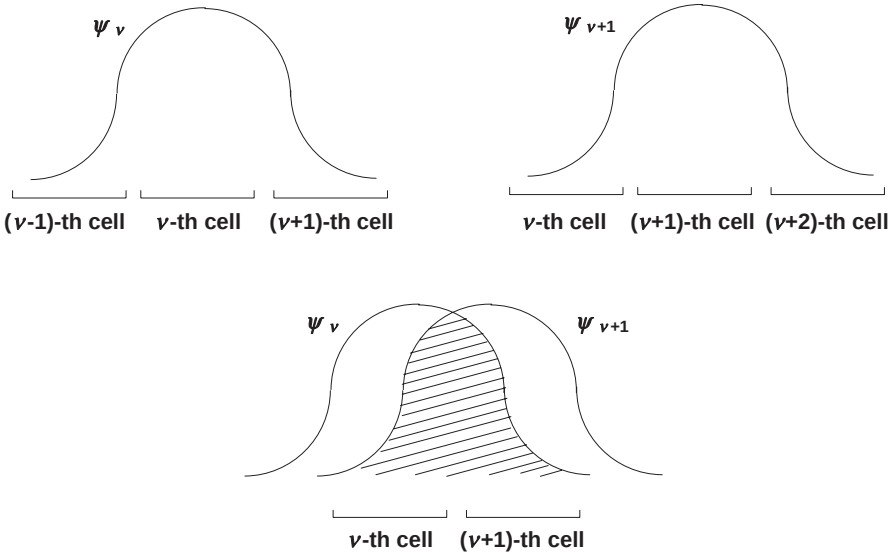

Figure 8. Degree of localization in the Wannier functions. The ν-th Wannier function ψ_ν is spread over $(\nu \pm 1)$-th cells. In ferromagnetic stacking modes, the ν-th and $(\nu+1)$-th Wannier-functions (ψ_ν and $\psi_{\nu+1}$) span common atoms between ν-th and $(\nu+1)$-th cells.

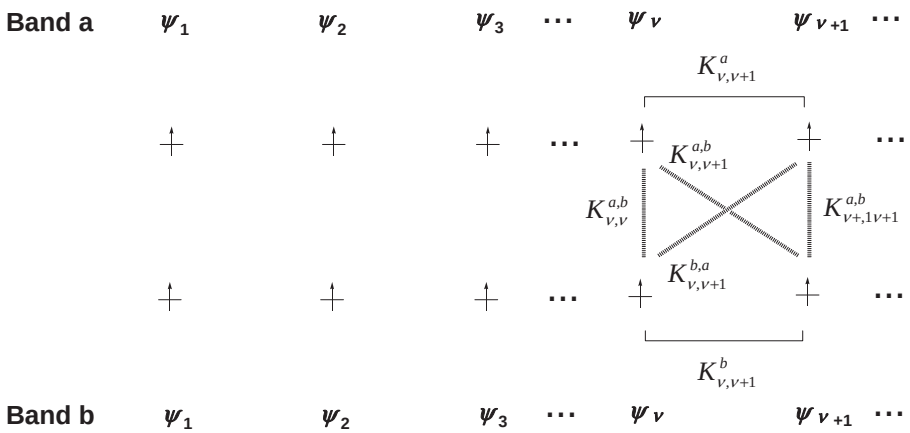

Figure 9. Electronic configuration of ferromagnetic states in organic-radical assemblies.

The electronic configuration of the ferromagnetic state of **5** is described in Figure 9. We note that there are two degenerate NBCO bands "a" and "b" corresponding to the two independent Wannier functions. Then, the ferromagnetic interactions occur between two Wannier functions with different index ν in the same band, and all the index ν in the different band. However, taking account of interactions within the ν-th and $(\nu+1)$-th cells, we can describe qualitative descriptions of the ferromagnetism. The possible ferromagnetic interactions in the two bands are schematically shown in Figure 9. Each interaction between the ν-th and $(\nu+\delta)$-th cells creates exchange integral $K_{\nu,\nu+\delta}$. From eq 25, ferromagnetic interactions of more than two adjacent cells are considered to be trivial. Therefore, putting δ to be 0 or 1, we focus on amplitude pattern in the product of Wannier functions $\psi_\nu\psi_{\nu+\delta}$, which is an effective two-electron wave function consisting of the product of the ν-th and $(\nu+\delta)$-th Wannier functions.

This is constructed as $PNBCO_{\nu,\nu+\delta}$:

$$
\begin{aligned}
PNBCO_{\nu,\nu+\delta} = \psi_\nu(\boldsymbol{1})\psi_{\nu+\delta}(\boldsymbol{2}) &= \left(\sum_{\mu}^{N}\sum_{r}^{n} a_r(\mu-\nu)\chi_{\mu,r}(\boldsymbol{1})\right) \\
&\times \left(\sum_{\mu'}^{N}\sum_{s}^{n} a_s(\mu'-\nu-\delta)\chi_{\mu',s}(\boldsymbol{2})\right) \\
&= \left(\sum_{\tau+\nu}^{N}\sum_{r}^{n} a_r(\tau)\chi_{\tau+\nu,r}(\boldsymbol{1})\right) \\
&\times \left(\sum_{\tau'+\nu'}^{N}\sum_{s}^{n} a_s(\tau'-\delta)\chi_{\tau'+\nu,s}(\boldsymbol{2})\right) \\
&\cong \left(\sum_{\tau}^{-1,0,1}\sum_{r}^{n} a_r(\tau)\chi_{\tau+\nu,r}(\boldsymbol{1})\right) \\
&\times \left(\sum_{\tau'}^{-1+\delta,\delta,1+\delta}\sum_{s}^{n} a_s(\tau'-\delta)\chi_{\tau'+\nu,s}(\boldsymbol{2})\right)
\end{aligned}
$$

$$= \left[\sum_{r}^{n}\{a_r(-1)\chi_{\nu-1,r}(\boldsymbol{1}) + a_r(0)\chi_{\nu,r}(\boldsymbol{1}) + a_r(1)\chi_{\nu+1,r}(\boldsymbol{1})\}\right] \times \left[\sum_{s}^{n}\{a_s(-1)\chi_{\nu-1+\delta,s}(\boldsymbol{2}) + a_s(0)\chi_{\nu+\delta,s}(\boldsymbol{2}) + a_s(1)\chi_{\nu+1+\delta,s}(\boldsymbol{2})\}\right] \quad (26)$$

where eq 24 is applied in the approximation. The electron numbers "***1***" and "***2***" were added in bold letters for clarification. When the NDO approximation was applied, eq 26 is further approximated as follows:
when $\delta = 0$,

$$PNBCO_{\nu,\nu} \cong C\left[\begin{array}{l} \sum_{r}^{(\nu-1)\text{-th cell}}\{a_r(-1)^2\chi_{\nu-1,r}(\boldsymbol{1})\chi_{\nu-1,r}(\boldsymbol{2})\} \\ + \sum_{r}^{\nu\text{-th cell}}\{a_r(0)^2\chi_{\nu,r}(\boldsymbol{1})\chi_{\nu,r}(\boldsymbol{2})\} \\ + \sum_{r}^{(\nu+1)\text{-th cell}}\{a_r(1)^2\chi_{\nu+1,r}(\boldsymbol{1})\chi_{\nu+1,r}(\boldsymbol{2})\} \end{array}\right] \cong C\left[\sum_{r}^{\nu\text{-th cell}}\{a_r(0)^2\chi_{\nu,r}(\boldsymbol{1})\chi_{\nu,r}(\boldsymbol{2})\}\right] \quad (27)$$

when $\delta = 1$,

$$\begin{aligned} PNBCO_{\nu,\nu+1} &\cong C\left[\sum_{r}^{\nu\text{-th cell}}\{a_r(-1)a_r(0)\chi_{\nu,r}(\boldsymbol{1})\chi_{\nu,r}(\boldsymbol{2})\} + \sum_{r}^{(\nu+1)\text{-th cell}}\{a_r(0)a_r(1)\chi_{\nu+1,r}(\boldsymbol{1})\chi_{\nu+1,r}(\boldsymbol{2})\}\right] \\ &= C\left[\sum_{r}^{\nu\text{-th cell}}\{a_r(0)a_r(1)\chi_{\nu,r}(\boldsymbol{1})\chi_{\nu,r}(\boldsymbol{2})\} + \sum_{r}^{(\nu+1)\text{-th cell}}\{a_r(0)a_r(1)\chi_{\nu+1,r}(\boldsymbol{1})\chi_{\nu+1,r}(\boldsymbol{2})\}\right] \end{aligned} \quad (28)$$

where $a_r(\pm1)^2$ was ignored comparing with $a_r(0)^2$, because eq 25 was supposed.

In eq 28, even-function character of $a_r(\tau)$ (eq 23) was applied. The first and second summations are taken in the ν-th and $(\nu+1)$-th cell, respectively. C in each expressions is chosen so that $PNBCO_{\nu,\nu+\delta}$ is normalized under the NDO approximation. NDO approximation is useful for description of NBMO-degenerate systems.[16–18] These expressions makes it possible to obtain schematic representation of $PNBCO_{\nu,\nu+\delta}$ by simple product between the coefficients on the same atomic site in the ν-th and $(\nu+\delta)$-th cells. $PNBCO_{\nu,\nu+\delta}$ with $\delta \geqq 2$ is not important due to the high localization of the Wannier functions.

Since NDO approximation was applied, the $PNBCO_{\nu,\nu+\delta}$ contained only ionic terms, that is, $\chi_{\nu,r}(\boldsymbol{1})\chi_{\nu,r}(\boldsymbol{2})$ and $\chi_{\nu+1,r}(\boldsymbol{1})\chi_{\nu+1,r}(\boldsymbol{2})$. Therefore, the squared amplitudes of the $PNBCO_{\nu,\nu+\delta}$ represent instabilities of anti-parallel-spin states. In short, since simultaneous occupancy of two electrons with parallel spin at the same atomic orbital is forbidden by the Pauli principle, resultant reduction of Coulomb repulsion leads to parallel-spin preference in $PNBCO_{\nu,\nu+\delta}$. This situation resembles those in nondisjoint biradicals and ally-radical dimers described in the previous section, in which sums of the the squared amplitudes of PNBMOs represent singlet instabilities.[11,16] Therefore, apart from the normalization factor, the sum of the squared amplitudes of $PNBCO_{\nu,\nu+\delta}$ is considered to be approximately proportional to exchange integral between the two Wannier functions ψ_ν and $\psi_{\nu+\delta}$. Such a consideration is consistent with recent studies of non-Kekulé oligomers and/or polymers using the L_{ij} index.[11–13]

By using the Wannier-function coefficients, it is shown that the total exchange integral K in **5** is approximately proportional to the number of unit cells as follows:

$$\begin{aligned} K &= \sum_{\nu}^{\text{band a}}\sum_{\tau\neq0}K^{a}_{\nu,\nu+\tau} + \sum_{\nu}^{\text{band b}}\sum_{\tau\neq0}K^{b}_{\nu,\nu+\tau} + \sum_{\nu}^{\text{band a and b}}\sum_{\tau}K^{a,b}_{\nu,\nu+\tau} + \sum_{\nu}^{\text{band b and a}}\sum_{\tau}K^{b,a}_{\nu,\nu+\tau} \\ &\cong N\{K^{a}_{\nu,\nu+1} + K^{b}_{\nu,\nu+1} + K^{a,b}_{\nu,\nu+1} + K^{b,a}_{\nu,\nu+1}\} + NK^{a,b}_{\nu,\nu} \\ &\propto 2N\sum_{r}^{\nu\text{-th cell}}\{a_{r,a}(0)^2a_{r,a}(1)^2 + a_{r,b}(0)^2a_{r,b}(1)^2 + a_{r,a}(0)^2a_{r,b}(1)^2 + a_{r,b}(0)^2a_{r,a}(1)^2\} + N\sum_{r}^{\nu\text{-th cell}}a_{r,a}(0)^2a_{r,b}(0)^2 \\ &= N\sum_{r}^{\nu\text{-th cell}}[2\{a_{r,a}(1)^2 + a_{r,b}(1)^2\}\{a_{r,a}(0)^2 + a_{r,b}(0)^2\} + a_{r,a}(0)^2a_{r,b}(0)^2] \\ &= N \times \text{const} \end{aligned} \quad (29)$$

where exchange integrals within the ν-th and $(\nu+1)$-th cells were taken into account. The coefficient 2 is resulted from amplitude identity of the ν-th and $(\nu+1)$-th cells in $PNBCO_{\nu,\nu+1}$. Strictly speaking, Wannier functions in band "a" and "b" should be transformed by unitary matrix so as to minimize the exchange integrals due to their degeneracy. This will be approximately realized so that sum of all the terms are minimized by using the Aoki–Imamura method.[11] But, in this paper, we only emphasize that the exchange integral per unit cell is approximately constant due to the Wannier-coefficient dependence, as described above.

Figure 10 shows the amplitude pattern of ψ_ν, $\psi_{\nu+1}$, and *PNBCOs* of **5**. Of all the *PNBCOs*, only $PNBCO_{\nu,\nu+1}$ in the same band were shown for simplicity. In **5**, ψ_ν and $\psi_{\nu+1}$ are quasi nondisjoint because the product between them, that is, *PNBCOs* are not zero in band "a" and/or "b." Therefore, *PNBCOs* are rich in ionic terms. This is essentially the origin of ferromagnetism of **5**.

Next, as another example of the ferromagnetic stacking mode, the Wannier functions and *PNBCOs* of **6** were analyzed. When we focus only on the linkage of carbon atomic sites, it can be seen from Figure 11 that **6** is topologically identical to non-Kekulé-like skeleton **6′**. The unit cell contains six carbon atomic sites as shown in Figure 11. Analogous to **5**, The Bloch and Wannier functions of **6** was deduced as following:

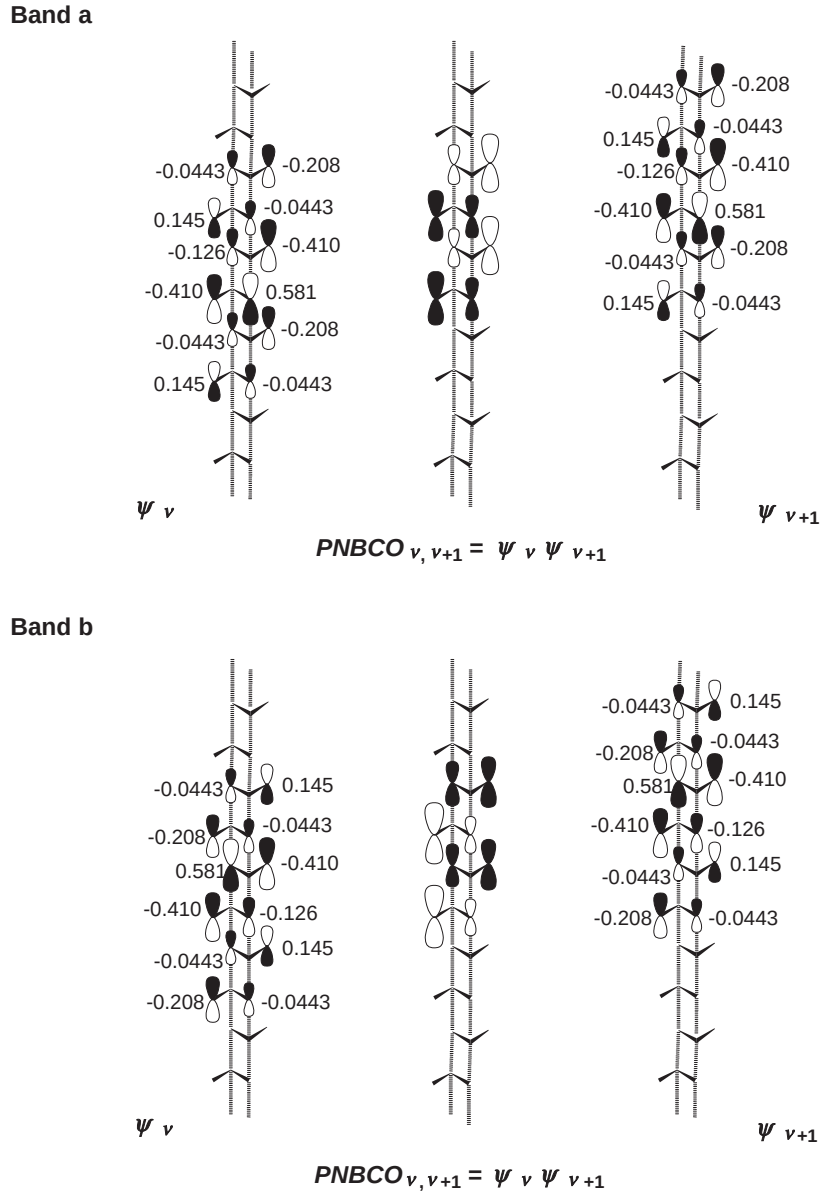

Figure 10. Schematic representation of the Wannier functions in **5**. Their product *PNBCOs* are also shown.

$$\begin{vmatrix} x & 1 & 0 & 0 & 0 & 0 \\ 1 & x & 1 & 1 & 0 & 0 \\ 0 & 1 & x & 0 & e^{ik} & 0 \\ 0 & 1 & 0 & x & 1 & 0 \\ 0 & 0 & e^{-ik} & 1 & x & 1 \\ 0 & 0 & 0 & 0 & 1 & x \end{vmatrix} = 0 \tag{30}$$

$$C_{1,a}(k) = -\frac{1}{\sqrt{2}}\frac{2}{\sqrt{8+2\cos k}},$$

$$C_{1,b}(k) = -\frac{1}{\sqrt{2}}\frac{2}{\sqrt{8+2\cos k}} \tag{31}$$

$$C_{2,a}(k) = C_{5,a}(k) = 0, \quad C_{2,b}(k) = C_{5,b}(k) = 0 \tag{32}$$

$$C_{3,a}(k) = \frac{1}{\sqrt{2}}\left\{\frac{1}{\sqrt{8+2\cos k}} + \frac{1}{\sqrt{4-2\cos k}}\right\},$$

$$C_{3,b}(k) = \frac{1}{\sqrt{2}}\left\{\frac{1}{\sqrt{8+2\cos k}} - \frac{1}{\sqrt{4-2\cos k}}\right\} \tag{33}$$

$$C_{4,a}(k) = \frac{1}{\sqrt{2}}\left\{\frac{1}{\sqrt{8+2\cos k}} - \frac{1}{\sqrt{4-2\cos k}}\right\},$$

$$C_{4,b}(k) = \frac{1}{\sqrt{2}}\left\{\frac{1}{\sqrt{8+2\cos k}} + \frac{1}{\sqrt{4-2\cos k}}\right\} \tag{34}$$

$$C_{6,a}(k) = \frac{1}{\sqrt{2}}\left\{-\frac{1+e^{-ik}}{\sqrt{8+2\cos k}} + \frac{1-e^{-ik}}{\sqrt{4-2\cos k}}\right\},$$

$$C_{6,b}(k) = \frac{1}{\sqrt{2}}\left\{-\frac{1+e^{-ik}}{\sqrt{8+2\cos k}} - \frac{1-e^{-ik}}{\sqrt{4-2\cos k}}\right\} \tag{35}$$

$$a_{1,a}(\tau) = -\frac{1}{\sqrt{2}}\frac{1}{2\pi}\int_{-\pi}^{\pi}\frac{2\cos(\tau k)}{\sqrt{8+2\cos k}}\,dk,$$

$$a_{1,b}(\tau) = -\frac{1}{\sqrt{2}}\frac{1}{2\pi}\int_{-\pi}^{\pi}\frac{2\cos(\tau k)}{\sqrt{8+2\cos k}}\,dk \tag{36}$$

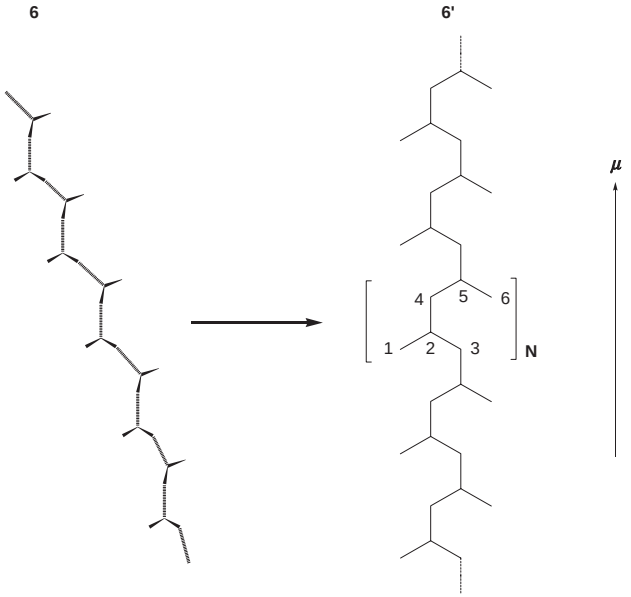

Figure 11. Carbon atomic linkage in **6**. The skeleton of **6** is formally reduced as **6′**.

$$a_{2,a}(\tau) = a_{5,a}(\tau) = 0, \quad a_{2,b}(\tau) = a_{5,b}(\tau) = 0 \tag{37}$$

$$a_{3,a}(\tau) = \frac{1}{\sqrt{2}}\left\{-\frac{1}{2}a_1(\tau) + \frac{1}{2\pi}\int_{-\pi}^{\pi}\frac{\cos(\tau k)}{\sqrt{4-2\cos k}}\,\mathrm{d}k\right\},$$

$$a_{3,b}(\tau) = \frac{1}{\sqrt{2}}\left\{-\frac{1}{2}a_1(\tau) - \frac{1}{2\pi}\int_{-\pi}^{\pi}\frac{\cos(\tau k)}{\sqrt{4-2\cos k}}\,\mathrm{d}k\right\} \tag{38}$$

$$a_{4,a}(\tau) = \frac{1}{\sqrt{2}}\left\{-\frac{1}{2}a_1(\tau) - \frac{1}{2\pi}\int_{-\pi}^{\pi}\frac{\cos(\tau k)}{\sqrt{4-2\cos k}}\,\mathrm{d}k\right\},$$

$$a_{4,b}(\tau) = \frac{1}{\sqrt{2}}\left\{-\frac{1}{2}a_1(\tau) + \frac{1}{2\pi}\int_{-\pi}^{\pi}\frac{\cos(\tau k)}{\sqrt{4-2\cos k}}\,\mathrm{d}k\right\} \tag{39}$$

$$a_{6,a}(\tau) = \frac{1}{\sqrt{2}}\left[\frac{1}{2}a_{1,a}(\tau) + \frac{1}{4}\{a_{1,a}(\tau+1) + a_{1,a}(\tau-1)\} + a_{3,b}(\tau) - \frac{1}{2}\{a_{3,b}(\tau+1) + a_{3,b}(\tau-1)\}\right],$$

$$a_{6,b}(\tau) = \frac{1}{\sqrt{2}}\left[\frac{1}{2}a_{1,a}(\tau) + \frac{1}{4}\{a_{1,a}(\tau+1) + a_{1,a}(\tau-1)\} - a_{3,b}(\tau) + \frac{1}{2}\{a_{3,b}(\tau+1) + a_{3,b}(\tau-1)\}\right] \tag{40}$$

The amplitude-pattern analysis is similarly described in Figure 12. From Figure 12, we can imagine that the *PNBCOs* also become ionic rich under the NDO approximation, because two localized NBCOs also span common atoms around the ν-th cells. Thus, this is also a quasi-nondisjoint polymer. This is the origin of ferromagnetism of **6**.

Finally, we analyze an antiferromagnetic organic-radical assemble **7**. The topological linkage is reduced as **7′** shown in Figure 13. Although the starred and unstarred atoms are linked to each other, this is predicted to be antiferromagnetic, as shown below. In contrast to the assemblies **5** or **6**, the unit cell of **7** can be chosen so as to contain only one allyl radical, because the formal skeleton **7′** consists of π–π stacking with an allyl-radical-moiety period. The unit cell is defined as shown in Figure 13.

The secular equation and NBCOs become:

$$\begin{vmatrix} x & 1+\mathrm{e}^{ik} & 0 \\ 1+\mathrm{e}^{-ik} & x & 1+\mathrm{e}^{-ik} \\ 0 & 1+\mathrm{e}^{ik} & x \end{vmatrix} = 0 \tag{41}$$

$$C_1(k) = -C_3(k) = \frac{1}{\sqrt{2}} \tag{42}$$

$$C_2(k) = 0 \tag{43}$$

These Bloch-function coefficients are independent of wavenumber k, and thus, the corresponding Wannier functions become:

$$a_1(\tau) = -a_3(\tau) = \frac{1}{2\pi}\int_{-\pi}^{\pi}\exp\{i(\mu-\nu)k\}\frac{1}{\sqrt{2}}\,\mathrm{d}k = \frac{1}{\sqrt{2}}\delta_{\mu\nu}\tau = (\mu-\nu) \tag{44}$$

$$a_2(\tau) = 0 \tag{45}$$

Thus, due to the Kronecker's delta, each Wannier function of **7** is localized only at one unit cell. This is schematically shown in Figure 14. Under the NDO approximation, each PNBCO vanishes, and thus, anti-parallel-spin instabilities are not deduced. When the NDO approximation was not applied, each PNBCO contains only covalent terms, which resembles valence-bond-type wave functions. In such a case, exchange integrals between each PNBCO become negative due to bonding interactions, similar to valence-bond theory. Thus, low-spin ground state is expected in **7**. Indeed, as is shown in the next section, density-functional-theory (DFT) calculations predicted the low-spin ground state of **7**.

Discussion

The total exchange integrals K in the ferromagnetic stacking modes are considered to be approximately proportional to the sum of the squared amplitudes of *PNBCOs*, as described above. K is considered to be proportional to the energy difference $\Delta E_{\mathrm{HS\text{–}LS}}$ between the highest-spin state and lowest-spin state, and monotonously increase with respect to N. In particular, when N is large, $\Delta E_{\mathrm{HS\text{–}LS}}$ will be well proportional to N. That is:

$$K \propto \Delta E_{\mathrm{HS\text{–}LS}} \propto N \tag{46}$$

Thus, we calculated high-spin stabilities of oligomers ($N = 2$, 4, 8, and 16) corresponding to **5** and **6** by DFT calculations, and N dependence of $\Delta E_{\mathrm{HS\text{–}LS}}$ was confirmed. The low-spin stability of **7** was also confirmed by the same method as a comparative example.

DFT Calculations. Figure 15a shows a plot of DFT-calculated $\Delta E_{\mathrm{HS\text{–}LS}}$ (kJ mol^{-1}) versus N for **5**. $\Delta E_{\mathrm{HS\text{–}LS}}$ was calculated at B3LYP/3-21G level of theory[20–22] by using Gaussian.[23] If the spin contamination is well removed, this level of theory is suitable for description of qualitative high-spin stabilities in NBMO-degenerate systems.[13] In the calculations, all the adjacent C–C and C–H lengths were fixed at 1.40 and 1.09 Å, respectively, and C–C–C angles were fixed at 120.0° within allyl-radical units and 90.0° between the unit-linking points. The distances between the allyl-radical centers were fixed at 1.40 Å. In the present case, all the spin-squared

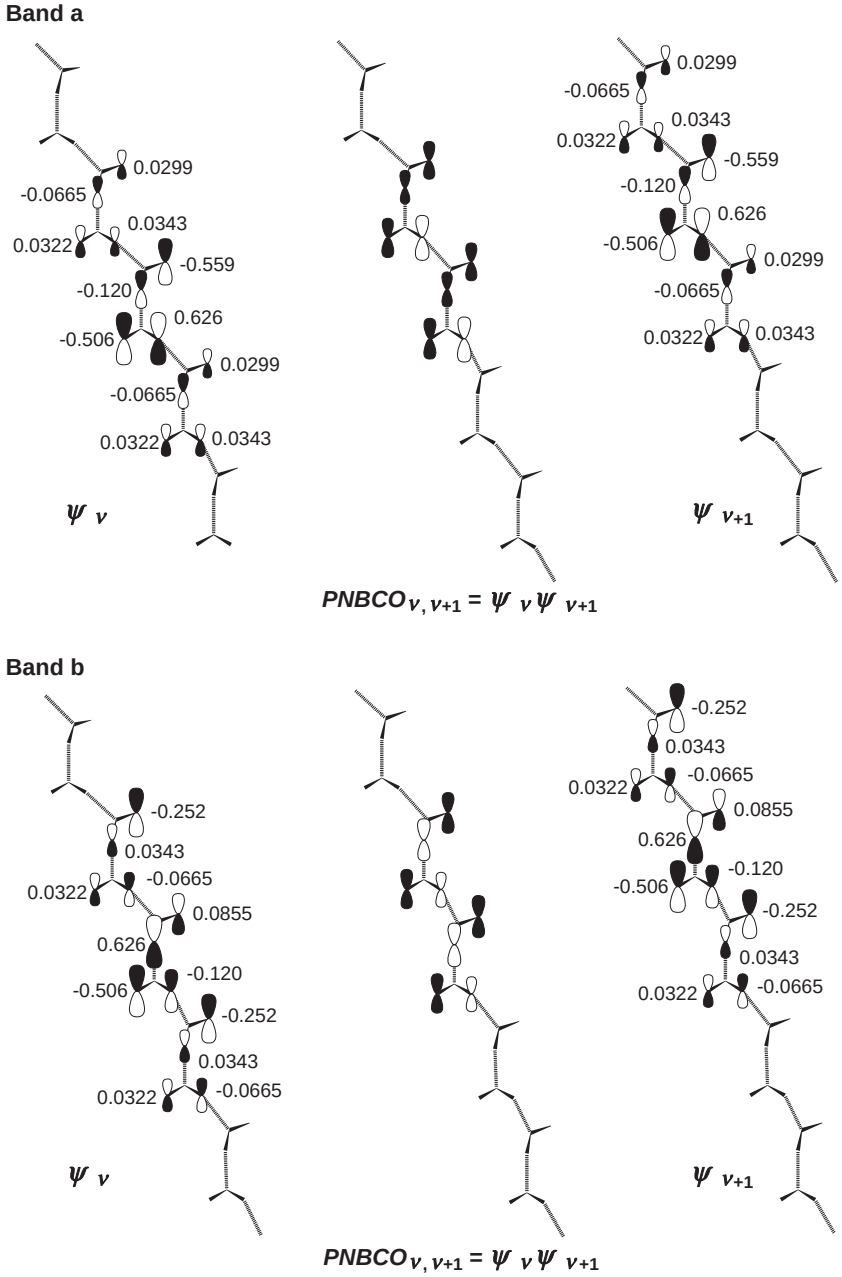

Figure 12. Schematic representation of the Wannier functions in **6**. Their product *PNBCOs* are also shown.

expectation values $\langle S^2 \rangle$ were almost purely obtained after annihilation, that is, $\langle S^2 \rangle = 2.0000$, 6.0025, 20.0039, and 72.0093 for high-spin states with $N = 2$, 4, 8, and 16, respectively. All the corresponding low-spin states were obtained as pure singlet with $\langle S^2 \rangle = 0.0000$. It can be seen from Figure 15a that $\Delta E_{\mathrm{HS-LS}}$ monotonously increases with N, and is approximately linear with respect to N. The deviation from linearity in small N is probably due to lack of enough size or some effects of the end groups. In large N ($>\approx 10$), we can expect high-spin stability proportional to N. The N-dependence of $\Delta E_{\mathrm{HS-LS}}$ is almost linear, because the essential amplitude pattern of $PNBCO_{\nu,\nu+\delta}$ is independent of ν, as seen from eq 26.

Next, a similar plot for polymer **6** is shown in Figure 15b. We obtained high-spin states with $\langle S^2 \rangle = 2.0000$, 6.0001, 20.0003, and 72.0006 for $N = 2$, 4, 8, and 16, respectively. All the corresponding low-spin states were also obtained as pure singlet with $\langle S^2 \rangle = 0.0000$. $\Delta E_{\mathrm{HS-LS}}$ was also linear with respect to large N. Since the amplitude pattern of each $PNBCO_{\nu,\nu+\delta}$ is also independent of ν, the N-dependence of $\Delta E_{\mathrm{HS-LS}}$ is also reasonable.

Finally, Figure 15c shows N-dependence of $\Delta E_{\mathrm{HS-LS}}$ in **7**. The high-spin states were obtained with $\langle S^2 \rangle = 2.0000$, 6.0002, 20.0006, and 72.0004 for $N = 2$, 4, 8, and 16, respectively. All the corresponding low-spin states were also obtained as singlet with $\langle S^2 \rangle = 0.0000$. It can be seen that this is a low-spin-preference polymer, because $\Delta E_{\mathrm{HS-LS}}$ decreases with N. In particular, when $N > 10$, this polymer clearly became antiferromagnetic. This is due to lack of high-spin stabilities in the *PNBCOs*, as formulated above. This is not only an

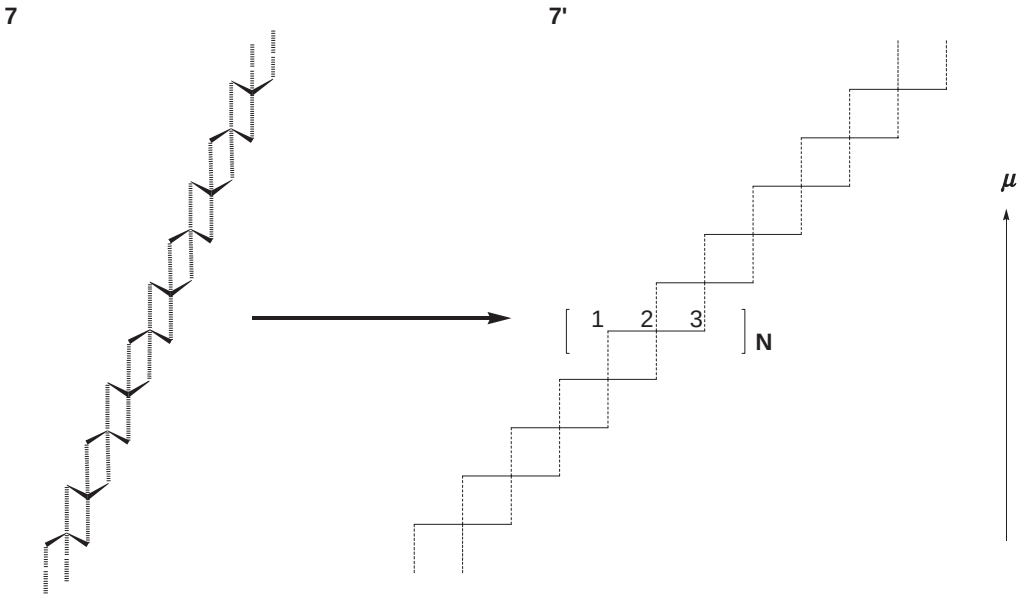

Figure 13. Carbon atomic linkage in **7**. The skeleton of **7** is formally reduced as **7′**.

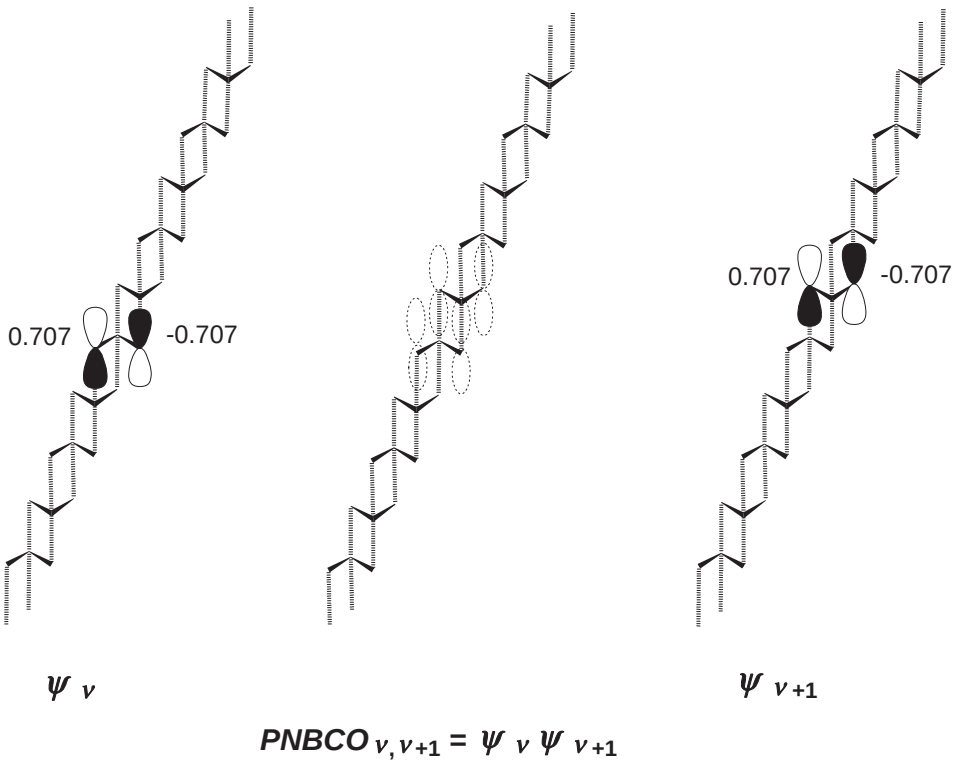

Figure 14. Schematic representation of the Wannier functions in **7**. Their product *PNBCOs* vanish under the NDO approximation.

interesting example in which a simple spin-polarization rule does not hold, but also an important organic-radical assemble, which supports our spin-preference analysis.

Conclusion

Ferromagnetic interactions in organic-radical assemblies were deduced under periodic boundary conditions. Although the topological-linkage patterns apparently contained pentavalent carbon atomic sites due to the three dimensionalities, it was shown that the degenerate non-bonding crystal orbitals (NBCOs) were subject to orbital mixing to form Wannier-transformed NBCOs, analogous to non-Kekulé polymers. Whereas in the ferromagnetic stacking modes the NBCOs were spread over more than two adjacent unit cells, in the antiferromagnetic stacking modes the NBCOs were localized only at one unit cell. High-spin preferences in the ferromagnetic stacking modes were attributed to anti-parallel-spin instabilities in effective two-electron wave functions consisting of

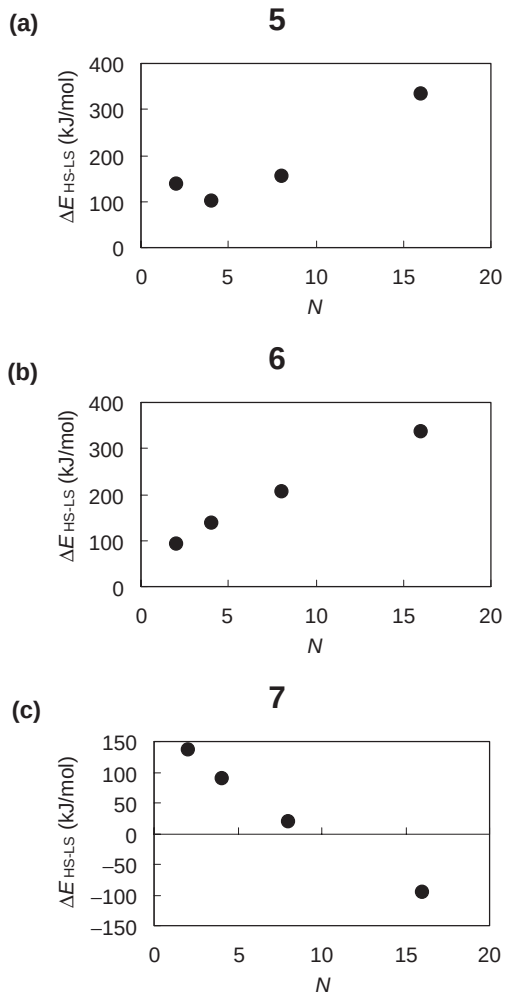

Figure 15. Relative high-spin stabilities ΔE_{HS-LS} (kJ mol^{-1}) in **5** (a), **6** (b), and **7** (c) at B3LYP/3-21G level of theory. The calculated ground-state energies for the dimers corresponding to **5** and **6** are −232.806839641 and −232.909933718 hartree, respectively, and for **7**, identical to that in **5**.

products of NBCOs (PNBCOs). Our analysis was supported by theoretical calculations.

References

1 H. C. McConnell, *J. Chem. Phys.* **1963**, *39*, 1910.
2 A. A. Ovchinnikov, *Theor. Chim. Acta* **1978**, *47*, 297.
3 K. Yamaguchi, T. Fueno, *Chem. Phys. Lett.* **1989**, *159*, 465.
4 K. Yamaguchi, Y. Toyoda, T. Fueno, *Chem. Phys. Lett.* **1989**, *159*, 459.
5 K. Tanaka, T. Takeuchi, K. Yoshizawa, M. Toriumi, T. Yamabe, *Synth. Met.* **1991**, *44*, 1.
6 A. Izuoka, S. Murata, T. Sugawara, H. Iwamura, *J. Am. Chem. Soc.* **1985**, *107*, 1786.
7 A. Izuoka, S. Murata, T. Sugawara, H. Iwamura, *J. Am. Chem. Soc.* **1987**, *109*, 2631.
8 H. Iwamura, *Adv. Phys. Org. Chem.* **1990**, *26*, 179.
9 K. Yoshizawa, R. Hoffmann, *J. Am. Chem. Soc.* **1995**, *117*, 6921.
10 K. Yoshizawa, T. Yamabe, R. Hoffmann, *Mol. Cryst. Liq. Cryst.* **1997**, *305*, 157.
11 Y. Aoki, A. Imamura, *Int. J. Quantum Chem.* **1999**, *74*, 491.
12 Y. Orimoto, T. Imai, K. Naka, Y. Aoki, *J. Phys. Chem. A* **2006**, *110*, 5803.
13 Y. Orimoto, Y. Aoki, *J. Chem. Theory Comput.* **2006**, *2*, 786.
14 W. T. Borden, E. R. Davidson, *J. Am. Chem. Soc.* **1977**, *99*, 4587.
15 W. T. Borden, *Mol. Cryst. Liq. Cryst.* **1993**, *232*, 195.
16 M. Hatanaka, R. Shiba, *Bull. Chem. Soc. Jpn.* **2007**, *80*, 1750.
17 M. Hatanaka, R. Shiba, *Bull. Chem. Soc. Jpn.* **2007**, *80*, 2342.
18 M. Hatanaka, R. Shiba, *Bull. Chem. Soc. Jpn.* **2008**, *81*, 460.
19 N. N. Tyutyulkov, S. C. Karabunarliev, *Int. J. Quantum Chem.* **1986**, *29*, 1325.
20 C. Lee, W. Yang, R. G. Parr, *Phys. Rev. B* **1988**, *37*, 785.
21 A. D. Becke, *J. Chem. Phys.* **1993**, *98*, 1372.
22 A. D. Becke, *J. Chem. Phys.* **1993**, *98*, 5648.
23 M. J. Frisch, G. W. Trucks, H. B. Schlegel, G. E. Scuseria, M. A. Robb, J. R. Cheeseman, V. G. Zakrzewski, J. A. Montgomery, Jr., R. E. Stratmann, J. C. Burant, S. Dapprich, J. M. Millam, A. D. Daniels, K. N. Kudin, M. C. Strain, O. Farkas, J. Tomasi, V. Barone, M. Cossi, R. Cammi, B. Mennucci, C. Pomelli, C. Adamo, S. Clifford, J. Ochterski, G. A. Petersson, P. Y. Ayala, Q. Cui, K. Morokuma, N. Rega, P. Salvador, J. J. Dannenberg, D. K. Malick, A. D. Rabuck, K. Raghavachari, J. B. Foresman, J. Cioslowski, J. V. Ortiz, A. G. Baboul, B. B. Stefanov, G. Liu, A. Liashenko, P. Piskorz, I. Komaromi, R. Gomperts, R. L. Martin, D. J. Fox, T. Keith, M. A. Al-Laham, C. Y. Peng, A. Nanayakkara, M. Challacombe, P. M. W. Gill, B. Johnson, W. Chen, M. W. Wong, J. L. Andres, C. Gonzalez, M. Head-Gordon, E. S. Replogle, J. A. Pople, *Gaussian 98, Revision A.11.2*, Gaussian, Inc., Pittsburgh PA, **2001**.